NJC

ROYAL SOCIETY OF CHEMISTRY

PAPER

View Article Online
View Journal | View Issue

Cite this: *New J. Chem.*, 2021, **45**, 4185

Synthesis of novel regioisomeric phenanthro[*a*]phenazine derivatives through the S_NAr strategy and their self-assembly into columnar phases†

Alakananda Patra,[a] K. Swamynathan[ab] and Sandeep Kumar *[ab]

Received 14th October 2020,
Accepted 20th January 2021

DOI: 10.1039/d0nj05042c

rsc.li/njc

The cyclocondensation reaction of triphenylene-1,2-diquinone with 1,2-diamino-4-nitrobenzene results in two regioisomers, and is succeeded by a nucleophilic substitution reaction with alkyl mercaptans. The synthesis of unsymmetrically substituted phenazines, separation and characterization of their regioisomers are rare in discotic liquid crystal chemistry. Here, we report for the first time the synthesis of two regioisomers of phenanthro[*a*]phenazine *via* a simple S_NAr substitution reaction. Separation of these regioisomers was achieved successfully *via* column chromatography and they were well characterized by spectroscopic analysis. Both the regioisomers were found to be mesomorphic. This study throws a lot of light on the S_NAr strategy for functionalizing diverse π-conjugated systems for various applications.

1. Introduction

The chemical structures of discotic liquid crystals (DLCs) are composed of central π-conjugated cores functionalized with various flexible tails around the periphery.[1] These one-dimensional columnar stacks of molecules have a stunning ability to self-organize into several two-dimensional lattices. These 2D macrostructures can either be self-assembled into least-ordered arrangements, thus forming a discotic nematic phase, or in a typical columnar fashion, which can later arrange into a hexagonal, rectangular, oblique or lamellar lattice. The self-assembly of these DLCs is due to the interplay of two attractive interactions, namely π–π attraction between the cores which provides the rigidity to the system and hydrophobic interaction between the tails which counterbalances the former from forming three-dimensional crystals in a certain temperature range.[2] The columnar structure exhibited by discogens has shown great potential in various semiconducting applications such as photoconductors, organic light emitting diodes, solar cells, *etc.*, because of their excellent property of one-dimensional charge transport through the columnar stack due to the long-range order.[3,4] The derivatives of heterocyclic π-conjugated systems which are known for their excellent photophysical properties have also been reported for their mesogenicity.[5] Expansion of π-conjugation by extending the core or by incorporating heteroatoms is observed to be effective for producing more stable materials with lower HOMO–LUMO gaps, higher temperature range mesophase and better charge carrier mobility.[6]

Out of the numerous carbocyclic and heterocyclic DLCs reported in the literature,[7–9] triphenylene is one of the most notable discotic liquid crystalline cores,[10,11] thanks to its wonderful thermal stability, accessible chemistry and reasonable charge carrier mobility. Over the years, triphenylene cores have been heavily studied and diversified by fusing with different heteroatoms through numerous synthetic strategies leading to novel π-extended discotic core structures.[12–14] It has been documented that the introduction of nitrogen atoms into the aromatic core is an effective strategy for increasing the electron-withdrawing character and endowing the discotic central core with n-type characteristics.[15–18] Phenazines are well known heterocyclic moieties in the organic material literature for their numerous semiconducting and biological applications.[19,20] The synthesis of phenazines is often accomplished through the cyclocondensation of 1,2-diketones with 1,2-diamines in the presence of acid or base. Phenazine dyes have also shown excellent electronic properties.[21–27] There are many literature reports on mesogens based on the phenazine skeleton; besides, they have been shown to exhibit good hole-mobility and conducting behavior.[28–37] Our group has reported novel phenanthro[*a*]phenazine[38] and phenanthro[*b*]phenazine[39] DLCs in the past by the condensation of triphenylene-*o*-quinones with

[a] *Raman Research Institute, Soft Condensed Matter, C. V. Raman Avenue, Bangalore 560080, India. E-mail: skumar@rri.res.in; Fax: +91 80 23610492; Tel: +91 80 23610122*

[b] *Department of Chemistry, Nitte Meenakshi Institute of Technology (NMIT), Yelahanka, Bangalore 560064, India*

† Electronic supplementary information (ESI) available. See DOI: 10.1039/d0nj05042c

o-phenylenediamine. Our recent work on the charge mobility studies of these compounds suggests a similar hole mobility to that of hexakis(hexyloxy)triphenylene.[33]

The aromatic nucleophilic substitution reactions (S_NAr) have been the strategy to go for in the development of new organic materials in recent times.[40,41] There are many reports on the role of S_NAr reactions in the synthetic design of macrocycles, polymers, molecular cages and crosslinked network compounds.[42–50] The scope of this reaction is underexplored. The precursors needed for this synthetic strategy are both easily available and synthetically feasible. The halo derivatives are one of the mainly used precursors for the S_NAr pathway. This may be due to their good leaving ability as well as electron-withdrawing nature.[15] Apart from halogens, there are few reports on nitro[51] and cyano[52] groups being used in S_NAr reactions for making novel materials. In this report, we have adopted the nitro group for functionalizing phenanthro[*a*] phenazines through the S_NAr strategy with mercaptoalkyl chains mainly because of the cheaper cost of the precursor and easier purification.

In this work, we have used the S_NAr pathway to functionalize a nitro group containing phenanthro[*a*]phenazine with a mercaptoalkyl moiety. The synthesis of unsymmetrically substituted phenazines, and the separation and characterization of their regioisomers are rare in discotic liquid crystal chemistry. Here, we report for the first time the synthesis of two regioisomers of phenanthro[*a*]phenazine *via* a simple S_NAr substitution reaction. Separation of these regioisomers was achieved successfully by column chromatography and they were well characterized by spectroscopic analysis. The mercaptoalkyl substituted phenazines as well as the pre-final *i.e.* nitro functionalized phenanthro[*a*]phenazines self-assemble into the hexagonal columnar phase in a wide temperature range.

2. Results and discussion

2.1. Design and synthesis

The commercial pyrocatechol was alkylated using the Williamson synthetic conditions to form 1,2-bis(dodecyloxy)benzene (**2**). The obtained 1,2-bis(dodecyloxy)benzene was oxidatively trimerized through the Scholl reaction using ferric chloride ($FeCl_3$) which led to the desired 3,6,7,10,11-pentakis(dodecyloxy) triphenylene-2-ol as a by-product (**3**) along with 2,3,6,7,10,11-hexakis(dodecyloxy)triphenylene (**3′**). The 3, 6,7,10,11-pentakis (dodecyloxy)triphenylene-2-ol was separated from the reaction mixture using gravity column chromatography. Further oxidation of **3** in the presence of ceric ammonium nitrate gives rise to 3,6,7,10,11-pentakis(dodecyloxy)triphenylene-1,2-dione, which upon cyclo-condensation with commercially obtained 1,2-diamino 4-nitrobenzene gives both **5(a)** and **5(b)** regioisomers. Both the regioisomers were successfully separated using gravity column chromatography and taken for the final step involving substitution with mercaptans. The structures of the obtained final products **6(a–c)** and **6i(a–c)** were assigned through NMR

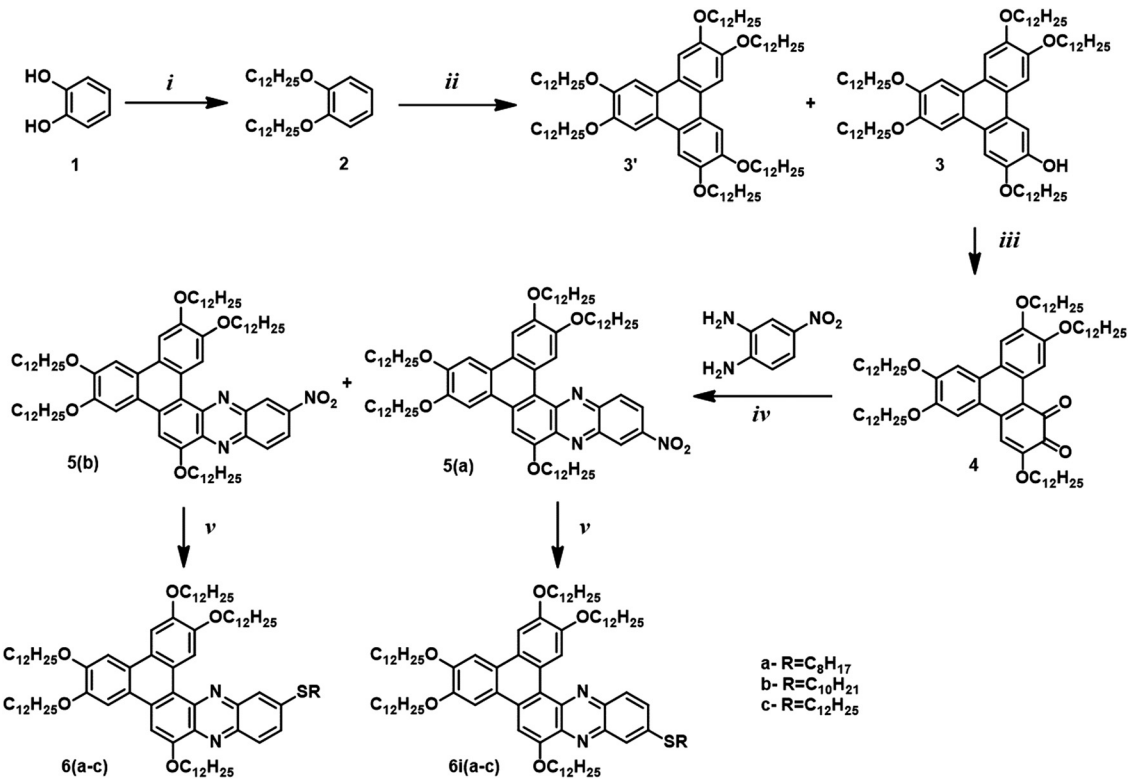

Scheme 1 Synthetic pathway of novel phenathro[*a*]phenazine derivatives (i) alkyl halide, anhydrous K_2CO_3, ethanol, reflux, 36 h, (ii) $FeCl_3$, dry DCM, room temperature, 1 h, (iii) ceric ammonium nitrate, THF–dioxane mixture, room temperature, 3 h, (iv) toluene, acetic acid, reflux, 12 h, (v) alkanethiol, anhydrous K_2CO_3, dry DMF, reflux, 12 h.

techniques and elemental analysis. The synthetic procedure is shown in Scheme 1.

2.2. Assignment of the structure of regioisomers through NMR analysis

The structures of both the regioisomers were assigned by the combination of both 1D and 2D NMR techniques. Assignment of the protons arranged in an ABX fashion, namely H_d, H_c and H_b, is mainly done using the ^{1}H NMR technique. In both the isomers **6i(b)** and **6(b)**, H_c and H_d undergo ortho coupling with a J of value around 9–9.5 Hz and H_b interacts with H_d with a smaller coupling constant (J around 1–1.5 Hz), giving rise to a doublet of doublets. The doublet for a single proton with J around 9 Hz is H_c and J around 1.5 Hz is H_b. Other protons are assigned to the peaks using ^{1}H and COSY NMR spectra (Fig. S5–S8, ESI†).

The ROESY experiment was used to ascertain the structure of regioisomers because a weak signal was expected between H_a and H_c in **6i(b)**, and also between H_a and H_b in **6(b)** due to their proximity in space. Fig. 1 shows the proton NMR and the corresponding ROESY spectrum of **6i(b)**. The most deshielded proton H_a shows a correlation with H_c (peak around δ = 8 ppm, doublet with J = 9 Hz) which signifies the spatial proximity between both, hence proving that the structure assigned is correct.

Fig. 2 shows the proton NMR and the corresponding ROESY spectra of compound **6(b)**. On analysing the ROESY spectrum of compound **6(b)**, proton H_a shows a correlation with H_b (peak around δ = 8 ppm, doublet with J = 1.5 Hz) which matches with structure **6(b)**.

2.2. Mesomorphic and thermal properties

The primary indication of mesomorphism was realized from the observation of distinct liquid crystalline textures under polarized optical microscopy (POM)[53] and the double melting points from differential scanning calorimetry (DSC).[54,55] The exact values of phase transition as well as the corresponding enthalpy values were obtained from DSC measurements and the phases were confirmed using X-ray diffraction studies.

2.2.1. Polarized optical microscopy. The thermotropic behavior of all the prefinal **5(a–b)** and final **6i(a–c)** and **6(a–c)** compounds was first examined by polarising optical microscopy (POM) in both heating and cooling cycles by placing a small amount of compound between a normal glass slide and coverslip. The prefinal compounds **5(a)** and **5(b)** showed dendritic and mosaic textures respectively (Fig. 3), which suggests the presence of the columnar mesophase. The POM textures of the

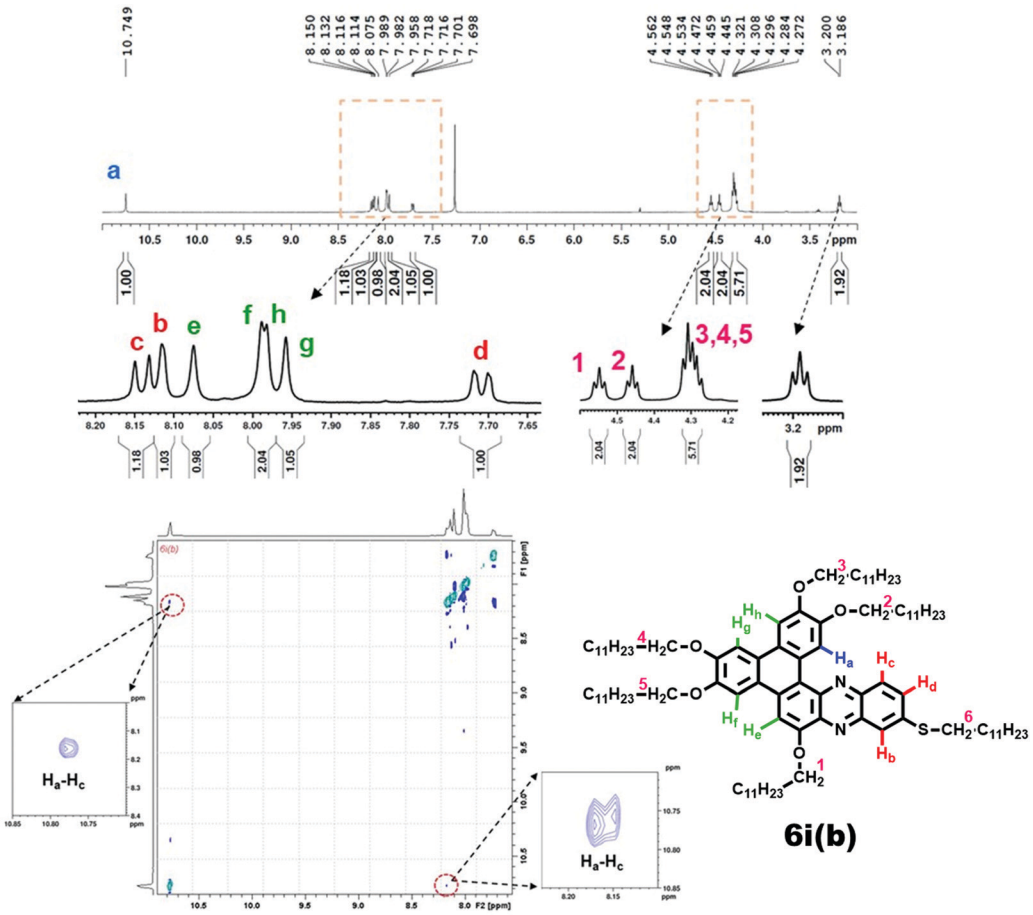

Fig. 1 ^{1}H and ROESY NMR spectra of compound **6i(b)**.

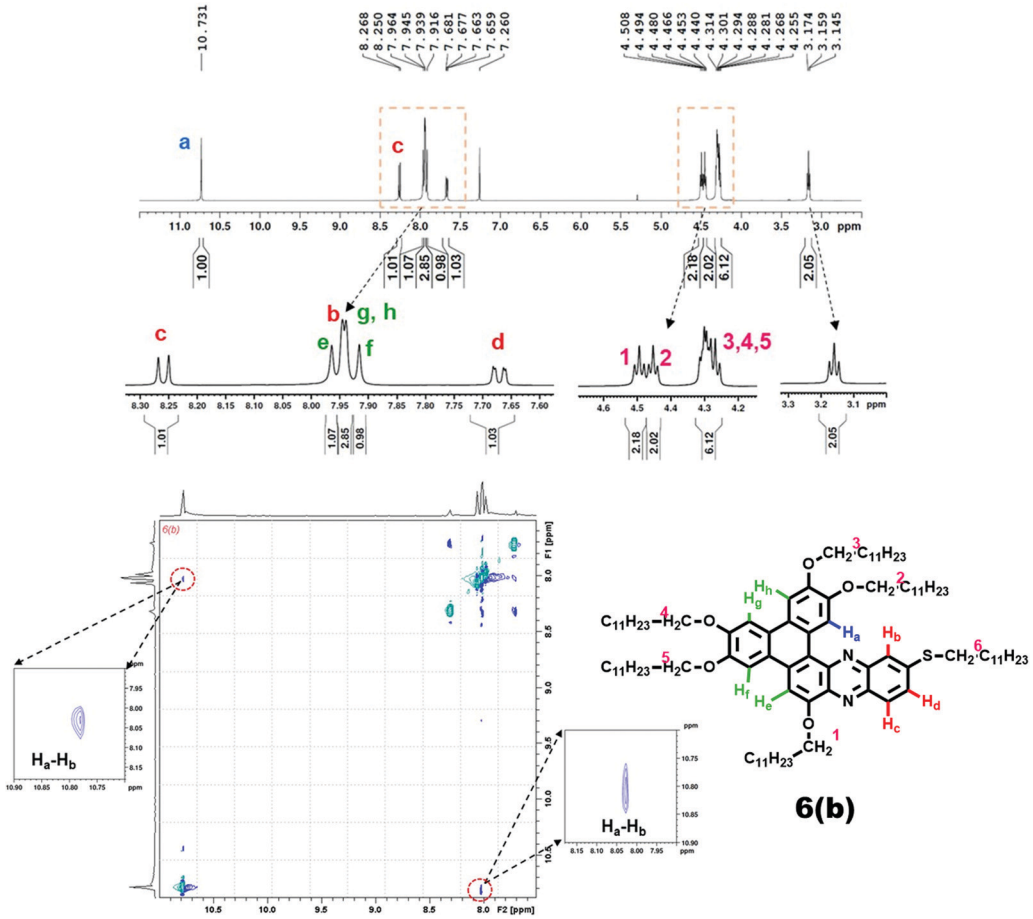

Fig. 2 ^{1}H and ROESY NMR spectra of compound **6(b)**.

final compounds **6(a–c)** and **6i(a–c)** are found to be exhibiting mosaic textures under crossed polarisers (Fig. 3 and Fig. S1, ESI†). These mosaic textures with rectilinear defects suggest that the final compounds show columnar mesophase as well.

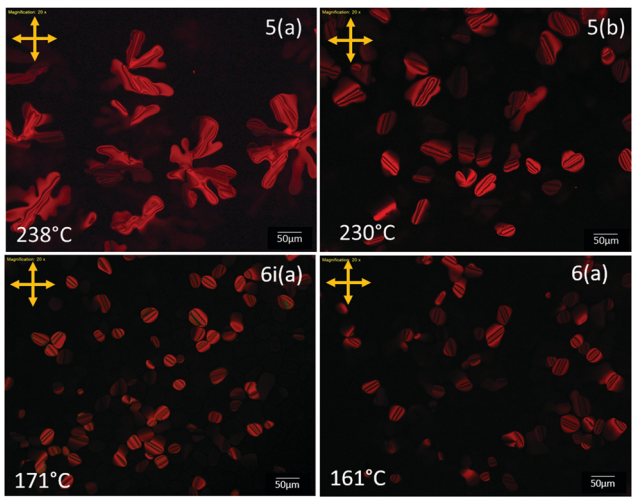

Fig. 3 Polarising optical microscopy textures: dendric textures of **5(a)** and mosaic texture of **5(b)**, **6i(a)**, and **6(a)**.

2.2.2. Differential scanning calorimetry. The DSC measurements of all the mesomorphic samples on both heating and cooling scans are recorded under an inert atmosphere. The phase transition temperatures are in good agreement with POM observations. The thermal behavior of all the pre-final and final compounds is summarized in Table 1. The peak temperatures are given in °C and the numbers in parentheses indicate the phase transition enthalpy (ΔH) in kJ mol^{-1}.

DSC thermograms of all the compounds show two peaks corresponding to melting and clearing transitions respectively. In the heating cycle, the isomers **6i(a–c)** transit to the liquid

Table 1 Phase transition temperature (peak temperature in °C) and enthalpies (kJ mol^{-1}, in brackets) of compounds **5a**, **5b**, **6i(a–c)** and **6(a–c)** on heating and cooling cycles. Cr = crystalline phase; Col_h = hexagonal columnar phase; I = isotropic phase

	Heating cycle	Cooling cycle
5a	Cr 64.3 (42.4) Col_h 242.3 (4.4) I	I 236.2 (3.5) Col_h 12.6 (36.8) Cr
5b	Cr 12.2 (29.7) Col_h 236.0 (2.9) I	I 230.5 (3.7) Col_h 5.6 (30.7) Cr
6ia	Cr 48.0 (69.4) Col_h 178.9 (6.5) I	I 175.9 (6.2) Col_h 21.3 (71.8) Cr
6ib	Cr 44.9 (51.3) Col_h 176.7 (3.9) I	I 173.6 (4.4) Col_h 21.6 (61.7) Cr
6ic	Cr 45.7 (58.6) Col_h 172.9 (6.5) I	I 170.6 (6.9) Col_h 21.2 (69.6) Cr
6a	Cr 79.9 (65.6) Col_h 169.6 (4.7) I	I 166.9 (4.5) Col_h 49.7 (70.0) Cr
6b	Cr 79.2 (63.0) Col_h 170.8 (6.4) I	I 168.6 (6.4) Col_h 45.7 (67.8) Cr
6c	Cr 79.5 (44.8) Col_h 169.7 (5.6) I	I 166.7 (5.5) Col_h 52.4 (54.7) Cr

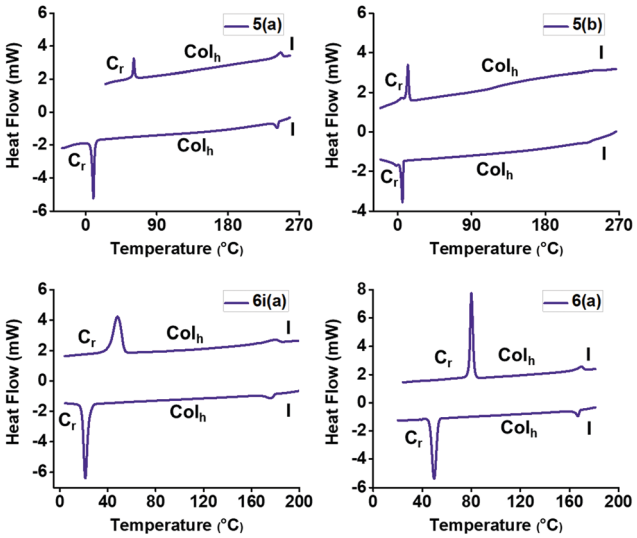

Fig. 4 DSC thermogram of compounds **5(a)**, **5(b)**, **6i(a)**, and **6(a)** at the scan rate of 10 °C min^{-1}.

crystal phase around 45 °C to 50 °C and completely melt around 170 °C to 180 °C. The second isomers **6(a–c)** melt around 79 °C to the liquid crystal phase, and they go to the isotropic phase around 170 °C. Further, in the cooling cycle, they crystallize at around 43 °C to 50 °C. Upon comparing with the previous reports from our group (compounds containing two thio-alkyl chains) these compounds show a higher clearing point which is because of a fewer number of flexible tails.[33] The details of the transition temperature and the associated enthalpy of all the prefinal and final compounds are listed in Table 1. DSC thermograms are shown in Fig. 4 and Fig. S3 (ESI†). The crystal to liquid crystal transition temperature of **5a** is 64 °C and its isotropic temperature is 242 °C, whereas **5b** shows the first transition at 12 °C and clearing temperature at 236 °C. This indicates that they are thermodynamically more stable among all our novel materials, because they possess the electron withdrawing nitro moiety, thereby decreasing the repulsion between the electron clouds originally expected in higher conjugated systems.[56]

2.2.3. Thermogravimetric analysis. The thermal stability of two compounds from each series of new materials was measured using thermogravimetric analysis (TGA) with a heat scan rate of 10 °C min^{-1} under an inert atmosphere. The compounds were found to be stable up to around 370 °C. The decomposition temperature was found to be around 480–500 °C which is much higher than the isotropic temperature indicating that the compounds possess good thermal stability, which in fact is the evidence of the suitability of our molecules for numerous application purposes. The representative TGA thermogram of the compounds is shown in Fig. S2 (ESI†).

2.2.4. X-Ray diffraction study. The columnar structure was further validated through X-ray diffraction. The diffractograms of the final compounds show the spacings of the low angle peaks in the ratio of $1:1/\sqrt{3}:1/2$ and can be indexed to a hexagonal lattice. Also, in the wide-angle region, two broad

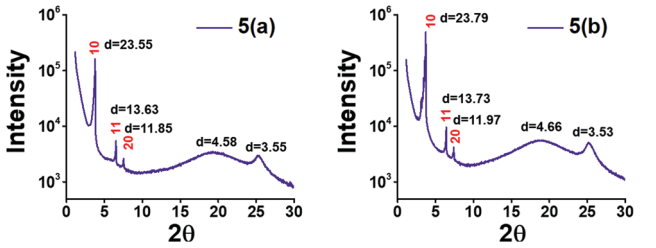

Fig. 5 XRD diffractograms of **5(a)** at 120 °C and **5(b)** at 130 °C (intensity in arbitrary unit and *d* spacing in Å).

peaks are observed, of which one is associated with the fluid nature of the alkyl chains and the other is due to the interaction between the cores. The representative X-ray diffraction patterns of all the mesogens are shown in Fig. 5, 6 and Fig. S4 (ESI†) and data are summarized in Table 2.

The diffractograms of the prefinal (**5a**, **5b**) and the final (**6ia–c**, **6a–c**) compounds show small-angle peaks in the ratio corresponding to that of a hexagonal lattice, which confirms the columnar hexagonal arrangements of all the novel materials. From the diffraction results, we have shown the number of molecules occupying one slice of a column to be around 1. Based on this we propose the following model for the arrangement of these compounds in their mesophase (Fig. 7).

2.3. Photophysical properties

The optical properties of all the final compounds were studied using UV-vis and fluorescence spectrometry (Fig. 8). The absorption spectra of compounds **6i(a–c)** exhibited four absorption peaks at 288 nm, 307 nm, 394 nm and 462 nm whereas the absorption spectra of compounds **6(a–c)** exhibited six absorption peaks at 264 nm, 285 nm, 307 nm, 348 nm, 411 nm and 450 nm. The emission spectra displayed a single peak for the isomer set **6i(a–c)** at 615 nm, 616 nm and 617 nm for **6ia**, **6ib**, and **6ic** respectively and for isomer set **6(a–c)** at 616 nm for all the compounds.

The absorptions (λ_{max}) of **6i(a–c)** isomers at 394 nm and 462 nm correspond to the n–π* and π–π* transitions and the peaks at 288 nm and 307 nm are possibly because of π–π* transitions of aromatic rings of the phenazine extended triphenylene core.

In the case of the second set of isomers **6(a–c)**, the absorption at 411 nm and 449 nm correspond to n–π* and π–π* transitions and the less intense peaks at 264 nm, 285 nm, 307 nm and

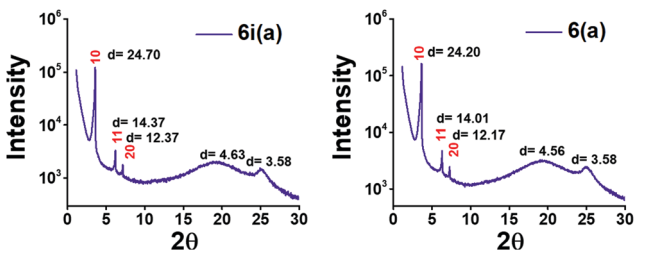

Fig. 6 XRD diffractograms of compounds **6i(a)** at 125 °C and **6(a)** at 90 °C (intensity in arbitrary unit and *d* spacing in Å).

Table 2 X-ray diffraction data for all mesomorphic compounds (a = lattice parameter = $\sqrt{(4/3)} \times d_{10}$; lattice area $A = S_h = a^2 \sin 60^\circ$; lattice volume $V_h = a^2 \sin 60^\circ \times h_c$ (h_a if h_c is not observed); no. of molecules per slice of column (Z) = $(\sqrt{3} \times N_a \times \rho \times a^2 \times h)/2M$; N_a = Avogadro number; ρ = density in kg m^{-3}; a = lattice parameter; h_c = core core peak (h_a if core–core is not observed); M = molecular weight in kg m^{-3}, ρ = 1000 kg m^{-3})

	Phase	Spacing (Å) d_{obs}	d_{cal}	Index	Lattice parameters
5a	Col_h (120 °C)	23.55	23.55	10	a = 27.19 Å
		13.63	13.59	11	A = 640.324 Å^2
		11.85	11.78	20	V = 2273.1519 Å^3
		4.58			Z = 1.05
		3.55			
5b	Col_h (130 °C)	23.79	23.79	10	a = 27.47 Å
		13.63	13.73	11	A = 653.503 Å^2
		11.97	11.89	20	V = 2306.8675 Å^3
		4.66			Z = 1.07
		3.53			
6ia	Col_h (125 °C)	24.70	24.70	10	a = 28.52 Å
		14.37	14.26	11	A = 704.3960 Å^2
		12.37	12.35	20	V = 2521.7379 Å^3
		4.63			Z = 1.08
		3.58			
6ib	Col_h (120 °C)	24.70	24.70	10	a = 28.52 Å
		14.37	14.26	11	A = 704.3960 Å^2
		12.44	12.35	20	V = 2486.5179 Å^3
		4.60			Z = 1.05
		3.53			
6ic	Col_h (125 °C)	25.25	25.25	10	a = 29.15 Å
		14.60	14.58	11	A = 735.859 Å^2
		12.61	8.42	20	V = 2634.3776 Å^3
		4.61			Z = 1.09
		3.58			
6a	Col_h (90 °C)	24.20	24.20	10	a = 27.94 Å
		14.01	13.97	11	A = 676.057189 Å^2
		12.17	12.10	20	V = 2420.28474 Å^3
		4.56			Z = 1.04
		3.58			
6b	Col_h (75 °C)	24.57	24.57	10	a = 28.37 Å
		14.14	14.19	11	A = 697.026522 Å^2
		12.37	12.29	20	V = 2453.53336 Å^3
		4.60			Z = 1.03
		3.52			
6c	Col_h (135 °C)	25.25	25.25	10	a = 29.16 Å
		14.60	14.58	11	A = 735.859 Å^2
		12.61	12.62	20	V = 2634.3776 Å^3
		4.61			Z = 1.09
		3.58			

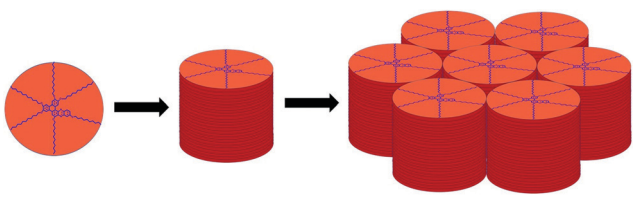

Fig. 7 Proposed arrangement of molecules of compounds **5a**, **5b**, **6(a–c)** & **6i(a–c)**; in the figure, the compound shown is **6ib**.

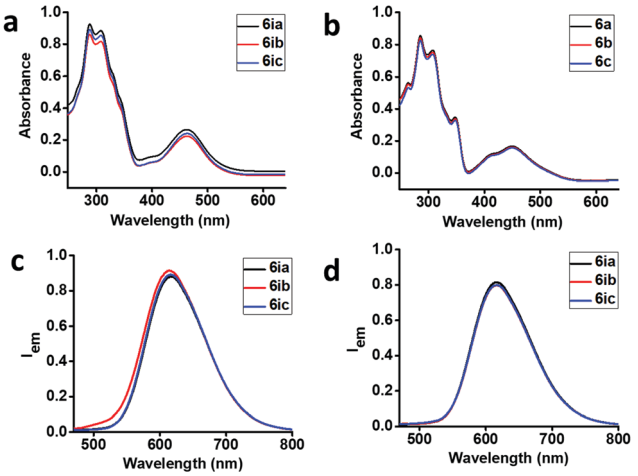

Fig. 8 (a) Absorbance spectra of **6i(a–c)**, (b) absorbance spectra of **6(a–c)**, (c) emission spectra of **6i(a–c)** excited at 460 nm, and (d) emission spectra of **6(a–c)** excited at 450 nm. All the compounds were dissolved in chloroform to obtain 7 μM concentration for recording the spectra.

348 nm are mostly because of the π–π* transitions of the aromatic core as the previous set of compounds.

The amount of light absorbed and the intensity of the peaks in the absorption spectrum generally depend on the extent of conjugation present in the discotic cores. On comparing with hexa-alkoxy triphenylene (λ_{max} = 300–400 nm), these systems show that a bathochromic shift of around 150 nm has occurred for both absorption and emission. This occurs due to the extension of conjugation in the central phenazine cores by three aromatic rings.

The Stokes shifts (the difference between the λ_{max} of absorption and emission) are 153 nm, 154 nm, and 155 nm for **6ia**, **6ib**, and **6ic** respectively and 167 nm for all the compounds of the **6(a–c)** series. λ_{onset} was determined by the intersection between the extrapolated tangent of the longest wavelength absorption peak and the x-axis and the optical energy gap (E_g) in eV was calculated according to the equation $E_g = 1240/\lambda_{onset}$. This along with the molar extinction coefficient data are summarized in Table 3. The absorbance and emission spectra of all the final compounds are shown in Fig. 8.

2. GAUSSIAN studies

Density functional theory (DFT) studies were carried out using the GAUSSIAN-09 program at Becke's three-parameter

Table 3 Molar extinction coefficient and the optical band gap of the compounds **6i(a–c)** and **6(a–c)**

Compound	Molar extinction coefficient (ε_{max}) (M^{-1} cm^{-1})	Optical bandgap ($1240/\lambda_{onset}$) (eV)
6ia	$\varepsilon_{462} = 1.85 \times 10^4$	2.31
6ib	$\varepsilon_{462} = 1.87 \times 10^4$	2.34
6ic	$\varepsilon_{462} = 1.89 \times 10^4$	2.35
6a	$\varepsilon_{450} = 1.77 \times 10^4$	2.35
6b	$\varepsilon_{450} = 1.69 \times 10^4$	2.36
6c	$\varepsilon_{450} = 1.60 \times 10^4$	2.38

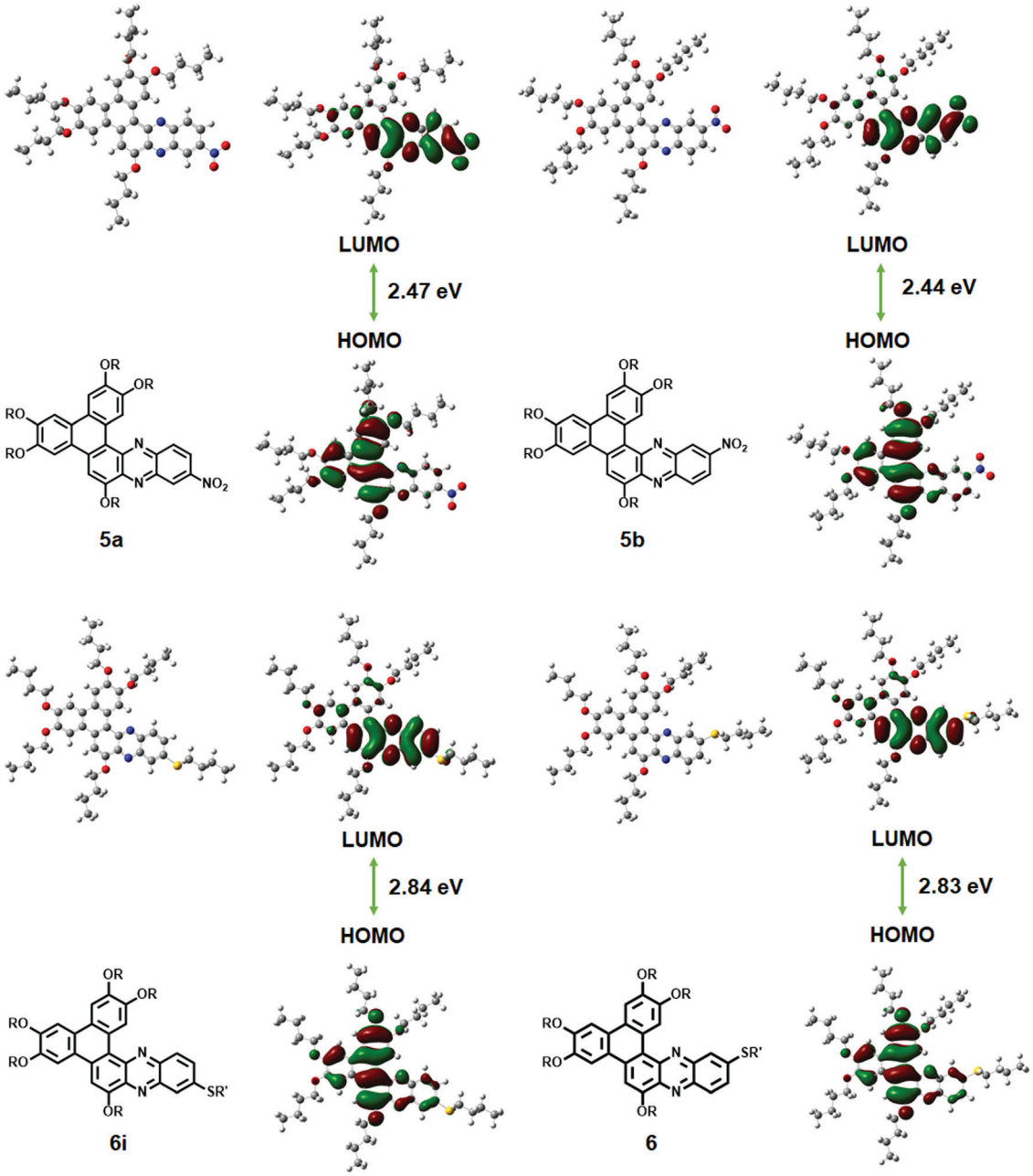

Fig. 9 Energy minimized structures, and HOMOs and LUMOs of **5a**, **5b**, **6**, and **6i**.

functional and the Lee, Yang and Parr correlation functional (DFT-B3LYP) by using the 6-31G(d) basis set.[38] The energy minimized structure of prefinal and final isomers and the HOMOs and LUMOs are given in Fig. 9. The energy gap was found to be 2.47 eV for the minimized structure of **5a** and 2.44 eV for the minimized structure of **5b**, 2.84 eV for the compounds of structure **6i** and 2.83 eV for compounds of structure **6**.

From the GAUSSIAN data, it was noticed that theoretically the net dipole moments of the structures assigned to molecule **6i** (3.6949 D) and **5a** (8.7233 D) are less than those of **6** (4.0655 D) and **5b** (12.1927 D) sequentially. This inference agrees with our observations that R_f values of **6i** and **5a** are larger than R_f values of **6** and **5b** respectively.

3. Conclusion

In our presented work, we have prepared two regioisomeric series of phenazine fused triphenylene-based compounds through the S_NAr strategy which are successfully separated *via* gravity column chromatography, thoroughly characterized and confirmed using both 1D and 2D NMR and theoretical calculations. The synthesized compounds and their precursors were found to be assembling in columns in their mesophase regime. The mesomorphic behaviour was analysed through the POM, DSC and XRD techniques. This S_NAr strategy can be one of the better alternatives in the expedition of the synthesis of novel organic materials. Furthermore, we are looking forward to

studying the charge transport and efficiency of these as semiconducting materials for practical applications.

4. Experimental section

The comprehensive synthetic procedure, and the spectral and elemental analysis data of all the intermediates can be found in the ESI.†

Synthesis of compounds 6i(a–c) & 6(a–c)

A mixture of compound **5(a)** or **5(b)** (1 eq.), potassium carbonate (4 eq.), and alkyl mercaptan (1.2 eq.) in dry DMF (10 ml per 1 g of compound **5**) was heated to 120 °C. The reaction was monitored using TLC. A saturated solution of sodium bicarbonate (20 vol%) was added to the reaction mixture after completion of the reaction. The mixture was extracted using dichloromethane and washed with brine. The organic layer was dried using anhydrous Na_2SO_4 and the solvent was removed under reduced pressure. The crude product was purified by column chromatography over silica gel using petroleum ether : ethyl acetate as the eluent (95 : 5). The isolated compounds were reprecipitated twice using DCM/MeOH to obtain a reddish-orange solid (60%).

Compound 6i(a). Orange solid, yield 60%, m.p. in Table 1, ^{1}H NMR: 10.733 (s, 1H), 8.116–8.101 (m, 2H), 8.039 (s, 1H), 7.962 (s, 2H), 7.936 (s, 1H), 7.706–7.685 (dd, 1H, J = 9, 2 Hz), 4.529 (t, 2H, J = 7 Hz), 4.446 (t, 2H, J = 7 Hz), 4.316–4.262 (m, 6H), 3.181 (t, 2H, J = 7.5 Hz), 2.184–1.272 (112H), 0.896–0.864 (m, 18H). ^{13}C NMR: 151.57, 150.76, 149.37, 148.80, 148.11, 143.81, 41.68, 140.62, 139.56, 137.37, 130.86, 129.85, 128.86, 126.61, 124.58, 123.14, 122.81, 118.39, 112.64, 108.15, 106.58, 105.92, 105.25, 69.92, 69.78, 69.29, 68.85, 32.33, 31.96, 31.83, 29.77, 29.72, 29.62, 29.41, 29.22, 29.20, 29.12, 28.96, 28.51, 26.38, 26.27, 26.24, 22.71, 14.13. Elemental analysis ($C_{92}H_{150}N_2O_5S$): C 79.14%, H 10.83%, N 2.01%, S 2.30% (expected); C 78.97%, H 11.16%, N 1.81%, S 1.91% (observed).

Compound 6i(b). Orange solid, yield 63%, m.p. in Table 1, ^{1}H NMR: 10.749 (s, 1H), 8.141 (d, 1H, J = 9 Hz), 8.11 (d, 1H, J = 1 Hz), 8.075 (s,1H), 7.989–7.982 (m, 2H), 7.958 (s, 1H), 7.718–7.698 (dd, 1H, J = 9, 1 Hz), 4.548 (t, 2H, J = 7 Hz) 4.459 (t, 2H, J = 6.5 Hz), 4.321–4.272 (m, 6H), 3.186 (t, 2H, J = 7 Hz), 2.205–1.271 (m, 116H), 0.876 (t, 18H, J = 7 Hz). ^{13}C NMR: 151.63, 150.81, 149.42, 148.85, 148.17, 143.83, 141.75, 140.68, 139.63, 137.43, 129.89, 128.88, 126.65, 124.97, 124.63, 123.16, 122.84, 118.46, 112.65, 108.22, 106.63, 105.98, 105.32, 69.97, 69.80, 69.55, 69.32, 68.88, 32.32, 31.95, 29.73, 29.71, 29.59, 29.41, 29.38, 29.33, 29.22, 29.10, 28.94, 28.51, 26.36, 26.25, 26.22, 22.71, 14.13. Elemental analysis ($C_{94}H_{154}N_2O_5S$): C 79.27%, H 10.90%, N 1.97%, S 2.25% (expected); C 78.76%, H 10.63%, N 1.75%, S 2.55% (observed).

Compound 6i(c). Orange solid, yield 65%, m.p. in Table 1, ^{1}H NMR: 10.74 (s, 1H), 8.127 (d, 1H, J = 9.5 Hz), 8.109 (d, 1H, J = 1.5 Hz), 8.055 (s, 1H), 7.972 (s, 2H), 7.946 (s,1H), 7.711–7.690 (dd, 1H, J = 9.5, 1.5 Hz), 4.537 (t, 2H, J = 7 Hz), 4.452 (t, 2H, J = 6.5 Hz), 4.317–4.266 (m, 6H), 3.183 (t, 2H, J = 7.5 Hz), 2.202–1.271 (120H), 0.877 (t, 18H, J = 6 Hz). ^{13}C NMR: 151.62, 150.80, 149.41, 148.84, 148.16, 143.83, 141.72, 140.68, 139.61, 137.43, 130.92, 129.88, 128.87, 126.64, 124.98, 124.62, 123.17, 122.83, 118.44, 112.65, 108.20, 106.63, 105.97, 105.31, 69.95, 69.80, 69.54, 69.31, 68.87, 32.32, 31.95, 29.77, 29.74, 29.71, 29.69, 29.68, 29.65, 29.62, 29.60, 29.56, 29.52, 29.49, 29.41, 29.39, 29.23, 29.11, 28.94, 28.51, 26.37, 26.26, 26.23, 22.71, 14.13. Elemental analysis ($C_{96}H_{158}N_2O_5S$): C 79.39%, H 10.97%, N 1.93%, S 2.21% (expected); C 79.35%, H 11.41%, N 1.70%, S 1.99% (observed).

Compound 6(a). Orange solid, yield 60%, m.p. in Table 1, ^{1}H NMR: 10.756 (s, 1H), 8.283 (d, 1H, J = 9.5 Hz), 7.062–7.952 (m, 5H), 7.701–7.679 (dd, 1H, J = 9.5, 1.5 Hz), 4.528 (t, 2H, J = 6 Hz), 4.477 (t, 2H, J = 6.5 Hz), 4.322–4.270 (m, 6H), 3.173 (t, 2H, J = 7.5 Hz), 2.211–1.272 (112H), 0.890–0.863 (m, 18H, J = 6 Hz). ^{13}C NMR: 151.84, 150.89, 149.38, 148.83, 148.09, 144.83, 142.09, 141.47, 138.76, 136.54, 130.62, 130.10, 129.73, 126.77, 125.08, 124.55, 122.81, 118.19, 112.55, 108.27, 106.72, 105.91, 104.56, 69.95, 69.84, 69.52, 69.29, 68.69, 32.38, 31.95, 31.84, 29.77, 29.72, 29.61, 29.57, 29.51, 29.41, 29.39, 29.26, 29.24, 29.15, 28.49, 26.52, 26.24, 22.71, 14.13. Elemental analysis ($C_{92}H_{150}N_2O_5S$): C 79.14%, H 10.83%, N 2.01%, S 2.30% (expected); C 78.88%, H 11.19%, N 1.38%, S 1.86% (observed).

Compound 6(b). Orange solid, yield 63%, m.p. in Table 1, ^{1}H NMR: 10.756 (s, 1H), 8.283 (d, 1H, J = 9.5 Hz), 7.964–7.939 (m, 5H), 7.692 (dd, 1H, J = 9.5, 1.5 Hz), 4.528 (t, 2H, J = 6 Hz), 4.477 (t, 2H, J = 6.5 Hz), 4.314–4.255 (m, 6H), 3.173 (t, 2H, J = 7.5 Hz), 2.196–1.272 (116H), 0.877 (t, 18H, J = 6 Hz). ^{13}C NMR: 151.82, 150.88, 149.38, 148.82, 148.08, 144.83, 142.07, 141.45, 138.74, 136.52, 130.61, 130.08, 129.71, 126.76, 125.09, 124.53, 122.81, 118.18, 112.56, 108.26, 106.71, 105.90, 104.54, 69.94, 69.84, 69.50, 69.29, 68.69, 32.39, 31.96, 31.91, 29.81, 29.77, 29.72, 29.65, 29.61, 29.52, 29.41, 29.39, 29.35, 29.31, 29.15, 29.01, 28.50, 26.53, 22.71, 22.69, 14.13, 14.11. Elemental analysis ($C_{94}H_{154}N_2O_5S$): C 79.27%, H 10.90%, N 1.97%, S 2.25% (expected); C 79.02%, H 11.15%, N 1.78%, S 1.92% (observed).

Compound 6(c). Orange solid, yield 63%, m.p. in Table 1, ^{1}H NMR: 10.740 (s, 1H), 8.269 (d, 1H, J = 9 Hz), 8.030–7.954 (m, 5H), 7.691 (dd, 1H, J = 9, 1.5 Hz), 4.528 (t, 2H, J = 7 Hz), 4.477 (t, 2H, J = 6.5 Hz), 4.296 (m, 6H), 3.173 (t, 2H, J = 7 Hz), 2.196–1.272 (120H), 0.877 (t, 18H, J = 6 Hz). ^{13}C NMR: 151.77, 150.85, 149.34, 148.78, 148.04, 144.80, 142.04, 141.42, 138.68, 136.46, 130.58, 130.06, 129.65, 126.73, 125.07, 124.50, 122.77, 118.13, 112.53, 108.20, 106.65, 105.85, 104.47, 69.91, 69.81, 69.46, 69.27, 68.67, 32.37, 31.96, 31.93, 31.60, 29.82, 29.77, 29.74, 29.72, 29.67, 29.62, 29.60, 29.59, 29.52, 29.43, 29.42, 29.40, 29.38, 29.33, 29.16, 29.01, 28.48, 26.54, 26.25, 22.72, 22.67, 14.13. Elemental analysis ($C_{96}H_{158}N_2O_5S$) S: C 79.39%, H 10.97%, N 1.93%, S 2.21% (expected); C 79.11%, H 11.19%, N 1.71%, S 1.93% (observed).

All synthesised compounds were characterised by ^{1}H and ^{13}C NMR and elemental analysis. Detailed spectra are also given in the ESI.†

Conflicts of interest

There is no conflict of interest.

Acknowledgements

The authors thank K. N. Vasudha for UV, DSC, XRD and elemental analysis; Dr H. T. Srinivasa for NMR and TGA measurements; Irla Sivakumar for valuable suggestions; Marichandran Vadivel, Vanishree Bhat and Ashwath N Gowda for their support and co-operation; Nancy Verma for help in PL studies and David Joseph for discussion regarding NMR analysis. We thank Prof. Victor Belyaev and Prof. Denis Chausov for helpful discussion. Department of Science and Technology, Government of India, Grant INT/RUS/RFBR/376 and Russian Foundation for Basic Projects, grant No. 19-57-45011_Ind_a are gratefully acknowledged.

References

1 S. Kumar, *Chemistry of discotic liquid crystals: from monomers to polymers*, CRC Press, New York, 2011.
2 S. Kumar, *Chem. Soc. Rev.*, 2006, **35**, 83–109.
3 S. Sergeyev, W. Pisula and Y. H. Geerts, *Chem. Soc. Rev.*, 2007, **36**, 1902.
4 S. Laschat, A. Baro, N. Steinke, F. Giesselmann, C. Hägele, G. Scalia, R. Judele, E. Kapatsina, S. Sauer, A. Schreivogel and M. Tosoni, *Angew. Chem., Int. Ed.*, 2007, **46**, 4832–4887.
5 M. Stępień, E. Gońka, M. Żyła and N. Sprutta, *Chem. Rev.*, 2017, **117**, 3479–3716.
6 B. Roy, N. De and K. C. Majumdar, *Chem. – Eur. J.*, 2012, **18**, 14560–14588.
7 H. K. Bisoyi and S. Kumar, *Liq. Cryst.*, 2011, **38**, 1427–1449.
8 S. Kumar, *Liq. Cryst. Today*, 2009, **18**, 2–27.
9 S. Kumar, *Liq. Cryst.*, 2009, **36**, 607–638.
10 S. Kumar, *Liq. Cryst.*, 2005, **32**, 1089–1113.
11 S. K. Pal, S. Setia, B. S. Avinash and S. Kumar, *Liq. Cryst.*, 2013, **40**, 1769–1816.
12 M. Vadivel, I. S. Kumar, K. Swamynathan, V. A. Raghunathan and S. Kumar, *ChemistrySelect*, 2018, **3**, 8763–8769.
13 A. R. Yuvaraj, A. Renjith and S. Kumar, *J. Mol. Liq.*, 2018, **272**, 583–589.
14 S. Kumar and S. K. Gupta, *Tetrahedron Lett.*, 2011, **52**, 5363–5367.
15 E. Keinan, S. Kumar, S. P. Singh, R. Ghirlando and E. J. Wachtel, *Liq. Cryst.*, 1992, **11**, 157–173.
16 I. Bala, H. Singh, V. R. Battula, S. P. Gupta, J. De, S. Kumar, K. Kailasam and S. K. Pal, *Chem. – Eur. J.*, 2017, **23**, 14718–14722.
17 I. Bala, S. P. Gupta, S. Kumar, H. Singh, J. De, N. Sharma, K. Kailasam and S. K. Pal, *Soft Matter*, 2018, **14**, 6342–6352.
18 S. Irla, V. A. Raghunathan and S. Kumar, *J. Mol. Liq.*, 2020, **314**, 113631.
19 A. R. Katritzky and C. W. Rees, *Comprehensive Heterocyclic Chemistry*, Elsevier, 1984.
20 V. K. Vishwakarma, S. Nath, M. Gupta, D. K. Dubey, S. S. Swayamprabha, J.-H. Jou, S. K. Pal and A. A. Sudhakar, *ACS Appl. Electron. Mater.*, 2019, **1**, 1959–1969.
21 N. Sato, *Six-Membered Hetarenes with Two Identical Heteroatoms*, Georg Thieme Verlag KG, 2004, p. 1.
22 A. B. Tathe and N. Sekar, *J. Fluoresc.*, 2015, **25**, 1403–1415.
23 A. H. Endres, M. Schaffroth, F. Paulus, H. Reiss, H. Wadepohl, F. Rominger, R. Krämer and U. H. F. Bunz, *J. Am. Chem. Soc.*, 2016, **138**, 1792–1795.
24 S.-S. Jester, E. Sigmund, L. M. Röck and S. Höger, *Angew. Chem., Int. Ed.*, 2012, **51**, 8555–8559.
25 J. Sun, Y. Sun, C. Yan, D. Lin, Z. Xie, S. Zhou, C. Yuan, H.-L. Zhang and X. Shao, *J. Mater. Chem. C*, 2018, **6**, 13114–13119.
26 Y. Sun, X. Li, C. Sun, H. Shen, X. Hou, D. Lin, H.-L. Zhang, C. Di, D. Zhu and X. Shao, *Angew. Chem., Int. Ed.*, 2017, **56**, 13470–13474.
27 W. Ratzke, L. Schmitt, H. Matsuoka, C. Bannwarth, M. Retegan, S. Bange, P. Klemm, F. Neese, S. Grimme, O. Schiemann, J. M. Lupton and S. Höger, *J. Phys. Chem. Lett.*, 2016, **7**, 4802–4808.
28 S. Chen, F. S. Raad, M. Ahmida, B. R. Kaafarani and S. H. Eichhorn, *Org. Lett.*, 2013, **15**, 558–561.
29 A. Gowda, L. Jacob, N. Joy, R. Philip and S. Kumar, *New J. Chem.*, 2018, **42**, 19034–19042.
30 A. Gowda, L. Jacob, A. Patra, A. George, R. Philip and S. Kumar, *Dyes Pigm.*, 2019, **160**, 128–135.
31 X. Crispin, J. Cornil, R. Friedlein, K. K. Okudaira, V. Lemaur, A. Crispin, G. Kestemont, M. Lehmann, M. Fahlman, R. Lazzaroni, Y. Geerts, G. Wendin, N. Ueno, J.-L. Brédas and W. R. Salaneck, *J. Am. Chem. Soc.*, 2004, **126**, 11889–11899.
32 C. W. Ong, S.-C. Liao, T. H. Chang and H.-F. Hsu, *Tetrahedron Lett.*, 2003, **44**, 1477–1480.
33 A. Gowda, L. Jacob, D. P. Singh, R. Douali and S. Kumar, *ChemistrySelect*, 2018, **3**, 6551–6560.
34 Y. He, S. Yagi, T. Maeda and H. Nakazumi, *Mol. Cryst. Liq. Cryst.*, 2015, **621**, 64–69.
35 P. Krzyczkowska, A. Krówczyński, J. Kowalewska, J. Romiszewski, D. Pociecha and J. Szydłowska, *Mol. Cryst. Liq. Cryst.*, 2012, **558**, 93–101.
36 C. W. Ong, C. Q. Yan, M.-C. Yeh and M.-C. Tzeng, *Mol. Cryst. Liq. Cryst.*, 2015, **610**, 249–254.
37 S. C. Mathur, B. Kumar and K. Roy, *Mol. Cryst. Liq. Cryst.*, 1979, **53**, 271–280.
38 S. Kumar and M. Manickam, *Liq. Cryst.*, 1999, **26**, 1097–1099.
39 S. Kumar and M. Manickam, *Mol. Cryst. Liq. Cryst. Sci. Technol., Sect. A*, 2000, **338**, 175–179.
40 J. F. Bunnett and R. E. Zahler, *Chem. Rev.*, 1951, **49**, 273–412.
41 F. Terrier, *Modern Nucleophilic Aromatic Substitution*, Wiley-VCH Verlag GmbH & Co. KGaA, Weinheim, Germany, 2013.
42 Q.-H. Guo, Z.-D. Fu, L. Zhao and M.-X. Wang, *Angew. Chem., Int. Ed.*, 2014, **53**, 13548–13552.
43 Z.-D. Fu, Q.-H. Guo, L. Zhao, D.-X. Wang and M.-X. Wang, *Org. Lett.*, 2016, **18**, 2668–2671.
44 Z.-C. Wu, Q.-H. Guo and M.-X. Wang, *Angew. Chem., Int. Ed.*, 2017, **56**, 7151–7155.

45 M. Jayakannan and S. Ramakrishnan, *Macromol. Rapid Commun.*, 2001, **22**, 1463.
46 Y. Xie, Q. Zhong, Y. Lv, J. Li, Z. Hao, C. Tang, X. Wei, Y. Su, J. Huang, A. Wang, X. Guo, J. Wang, G. Li and Y. Song, *ACS Appl. Mater. Interfaces*, 2019, **11**, 34203–34211.
47 W. Zou, J. Dong, Y. Luo, Q. Zhao and T. Xie, *Adv. Mater.*, 2017, **29**, 1606100.
48 J. W. Wackerly, M. Zhang, S. T. Nodder, S. M. Carlin and J. L. Katz, *Org. Lett.*, 2014, **16**, 2920–2922.
49 W. J. Ong and T. M. Swager, *Nat. Chem.*, 2018, **10**, 1023–1030.
50 T. M. Long and T. M. Swager, *J. Am. Chem. Soc.*, 2003, **125**, 14113–14119.
51 A. Kondoh, H. Yorimitsu and K. Oshima, *Tetrahedron*, 2006, **62**, 2357–2360.
52 O. Roussel, G. Kestemont, J. Tant, V. De Halleux, R. Gómez Aspe, J. Levin, A. Remacle, I. R. Gearba, D. Ivanov, M. Lehmann and Y. Geerts, *Mol. Cryst. Liq. Cryst.*, 2003, **396**, 35–39.
53 I. Dierking, *Textures of Liquid Crystals*, Wiley, 2003.
54 K. Ohta, H. Ema, H. Muroki, I. Yamamoto and K. Matsuzaki, *Mol. Cryst. Liq. Cryst.*, 1987, **147**, 61–78.
55 J. W. Goodby, *Handbook of Liquid Crystals*, Wiley-VCH Verlag GmbH & Co. KGaA, Weinheim, Germany, 2014, pp. 1–18.
56 E. J. Foster, R. B. Jones, C. Lavigueur and V. E. Williams, *J. Am. Chem. Soc.*, 2006, **128**, 8569–8574.

